Nano Research

ISSN 1998-0124 CN 11-5974/O4
https://doi.org/10.1007/s12274-021-3762-8

Research Article

Carbothermal shock enabled facile and fast growth of carbon nanotubes in a second

Haomin Wang[1,§], Huimin Wang[1,§], Shuchen Zhang[2], Yong Zhang[1], Kailun Xia[1], Zhe Yin[1], Mingchao Zhang[1], Xiaoping Liang[1], Haojie Lu[1], Shuo Li[1], Jin Zhang[2], and Yingying Zhang[1] (✉)

[1] *Key Laboratory of Organic Optoelectronics and Molecular Engineering of the Ministry of Education, Department of Chemistry, Tsinghua University, Beijing 100084, China*
[2] *Center for Nanochemistry, Beijing Science and Engineering Center for Nanocarbons, Beijing National Laboratory for Molecular Sciences, College of Chemistry and Molecular Engineering, Peking University, Beijing 100871, China*
[§] *Haomin Wang and Huimin Wang contributed equally to this work.*

Received: 31 May 2021 / **Revised:** 16 July 2021 / **Accepted:** 22 July 2021

ABSTRACT

Carbon nanotubes (CNTs) hold great promise in many fields because of their unique structures and properties. However, the preparation of CNTs generally involves cumbersome equipment and time-consuming processes. Here, we report an ultra-fast carbothermal shock (CTS) approach for synthesizing CNTs with a simple homemade setup by employing Joule heating of a carbon substrate. Carbonized silk fabric (CSF) loaded with transition metal salts in ethanol solution was used as the substrate, which was treated with a pulse voltage of 40 V for only 50 ms and then covered with uniform CNTs grown with bimetallic alloy catalyst nanoparticles (diameter: ~ 9 nm). The temperature ramp rate is as high as 10^5 K/s. The as-obtained sample has a unique fluffy structure similar to the trichobothrium of spiders, endowing it versatile applications such as airflow sensors or air filters. The CTS technique presents an easy-accessible and highly efficient approach for synthesizing CNTs, which may be also applied in synthesizing other nanomaterials.

KEYWORDS

carbothermal shock, Joule heating, carbon nanotube, ultra-fast growth, fluffy structure

1 Introduction

Carbon nanotubes (CNTs), which possess unique structures and properties, are of great interest for applications in various fields [1–10]. The efficient synthesis of high-quality CNTs is the basis for practical and wide applications of CNTs. Currently, there are three main methods for synthesizing CNTs, namely arc discharge [11, 12], laser ablation [13], and chemical vapor deposition (CVD) [1]. High-quality CNTs can be obtained by arc discharge and laser ablation, but these two approaches are accompanied by expensive equipment, low-yield, and multiple by-products. Besides, CVD, which has advantages of relatively simple setup, high-yield, and tunable morphology of the products [1, 9, 14, 15], is widely studied and adopted for synthesizing CNTs. The typically used catalysts include Fe, Co, Ni, Cu and their combination [16–18]. Despite the above advantages, it generally takes hours or even days to complete an entire CVD process for CNT growth due to the slow ramp rate (0.33 K/s) of usual CVD equipment [1, 15]. Therefore, it is still a big challenge to synthesize CNTs through a facile and highly efficient process with an easily accessible setup.

Recently, an interesting carbothermal shock (CTS) method was reported to produce high-entropy-alloy nanoparticles by employing flash heating and cooling of metal precursors on oxygenated carbon support [19]. On one hand, the CTS can provide the high temperature that is usually required for the growth of CNTs in a very short time through Joule heating. On the other hand, the as-formed metal nanoparticles with uniform structures may serve as high catalysts for the growth of CNTs. Therefore, we suspect that the facile and efficient growth of CNTs may be realized through a CTS process with selected precursors and optimized Joule thermal shock parameters.

In this work, we report the facile and ultra-fast growth of CNTs by employing ultra-fast Joule heating of carbonized silk fabric (CSF). The CSF was loaded with transition metal salts in ethanol solution. The temperature of CSF increased from room temperature to ~ 1,700 K with applying a pulse voltage of 40 V for only 50 ms, leading to the formation of uniformly distributed catalyst nanoparticles and *in-situ* growth of CNTs on the CSF fibers (CSF@CNTs). The synthesized CSF@CNTs showed a unique fluffy structure which is similar to the spider's trichobothrium, enabling it versatile functions. This CTS technique presents an easily accessible and highly efficient approach for the fast synthesis of CNTs and may also be valuable for growth of other nanomaterials.

2 Results and discussion

Figure 1(a) illustrates the CTS process for the growth of CNTs. Firstly, the ethanol solution containing two kinds of metal salts were dropped onto a piece of suspended CSF with a loading of 60

Address correspondence to yingyingzhang@tsinghua.edu.cn

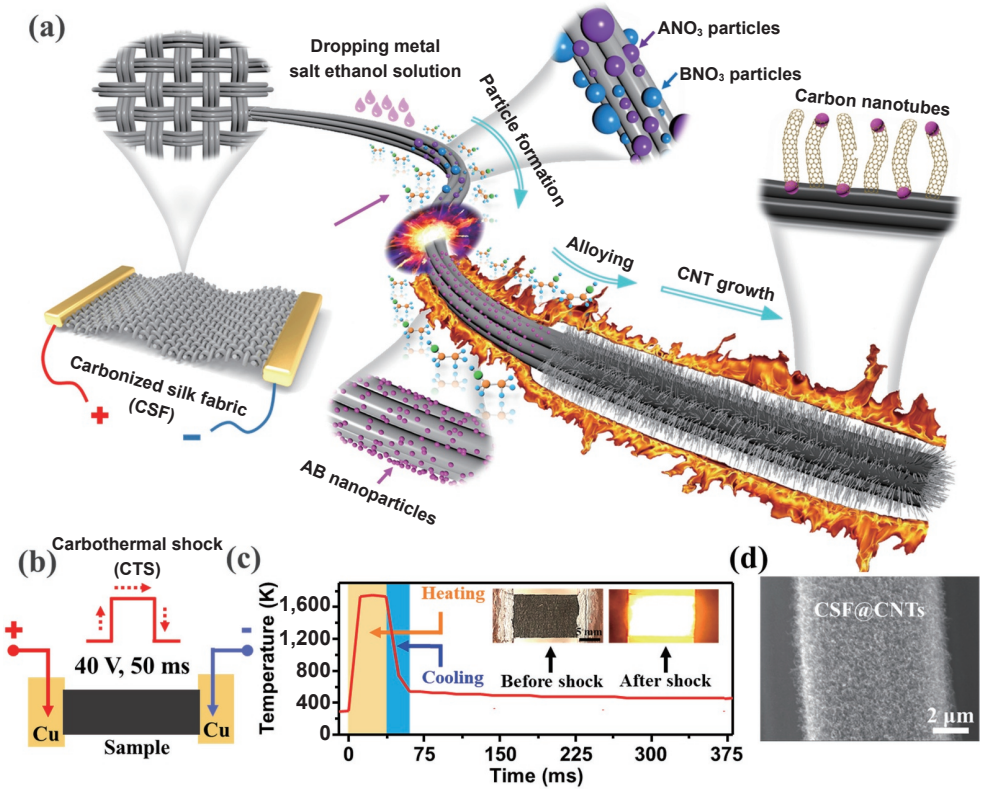

Figure 1 Carbothermal shock process for the growth of CNTs on a carbonized silk fabric. (a) Schematic illustration showing the CTS process. (b) Illustration showing the pulse voltage applied on the CSF. (c) Evolution of CSF temperature during the CTS process. (d) A scanning electron microscopy (SEM) image of the CSF@CNTs.

μL/cm^2. There, we typically used mixed ethanol solutions of two nitrate salts (Fig. S1 in the Electronic Supplementary Material (ESM)), such as $Co(NO_3)_2$-$Cu(NO_3)_2$, $Fe(NO_3)_3$-$Cu(NO_3)_2$, or $Ni(NO_3)_2$-$Cu(NO_3)_2$ (25 mM for each metal element), which were noted as ANO_3-BNO_3. $Co(NO_3)_2$-$Cu(NO_3)_2$ was used for the following samples unless otherwise noted. Then, the CSF was immediately put in a small Ar-filled household plastic storage box (polypropylene, 22 cm × 14 cm × 16 cm) and Joule heated to a high temperature by applying a pulse voltage. Instantaneously, high density, radially and uniformly distributed CNTs were grown on the CSF fibers.

The CTS temperature and duration can be easily controlled by tuning the electrical pulse parameters. Typically, we used an optimized voltage of 40 V for 50 ms (Fig. 1(b)), leading to an instant ramp of temperature to ~ 1,700 K with a heating rate of ~ 10^5 K/s (Fig. 1(c)). As shown in the inset of Fig. 1(c), bright light will instantly emit from the CSF (a gray body radiation source with the emissivity of ~ 0.8) [20, 21] when a constant voltage is applied, indicating the high temperature of the CSF as a result of Joule heating (Fig. S2 in the ESM). Simultaneously, fluffy CNTs were uniformly formed on the surface of the CSF fiber after the CTS process (Fig. 1(d)). It is worth noting that ethanol not only serves as a solvent of the catalyst precursor but also serves as the carbon precursor in the CTS process. A control experiment was carried out with dried CSF loaded with the metal precursor but free of ethanol and no CNT was observed after the same CTS process (Fig. S3 in the ESM).

We studied the evolution of CSF temperature during the CTS process and characterized the obtained CSF@CNTs. There are two main parameters that can be adjusted in the CTS process: the voltage and the pulse duration. A low voltage of 20 V cannot lead to the formation of alloy catalyst nanoparticles so that CNTs cannot be grown (Fig. S4(a) in the ESM); a high voltage of 60 V will cause the broken CSF substrate (Fig. S4(b) in the ESM). Therefore, we used the optimized voltage of 40 V. The evolution of temperature (Fig. S5(a) in the ESM) was tracked using a laser temperature gun while applying a pulse voltage of 40 V for different durations (from 50 ms to 10 s). As shown in Fig. 2(a), all the maximum temperatures are around 1,700 K for different CTS durations. Similar CNT morphology was observed for samples obtained with the same CTS process but different electrical pulse durations (Figs. 2(b) and 2(c), and Fig. S5(c) in the ESM). It is worth noting that 50 ms is the minimum value of time that our electric power source can achieve, indicating that the CTS process for growing CNTs can be completed in 50 ms or less. The obtained CNTs are multi-walled CNTs with diameters around 12.6 ± 0.95 nm and lengths around 1.5 ± 0.88 μm (Fig. 2(d) and Fig. S6 in the ESM). The Raman intensity ratio of D-band to G-band (I_D/I_G) of the CSF@CNTs (0.56) is smaller than that of the pristine CSF (1.04), while a new 2D peak centered at 2,700 cm^{-1} appears after the CTS process (Fig. 2(e), and Fig. S5(b) in the ESM), indicating the formation of high-quality CNTs. It should be noted that we have also tried to grow single-walled CNTs through the CTS process although we have not found the suitable conditions yet. The growth of CNTs on the CSF and the improved graphitization of CSF (Fig. S7 in the ESM) lead to increased conductance of the CSF@CNTs. As shown in Fig. 2(f), the conductance of the CSF@CNTs is 16.5 times that of the pristine CSF.

Figure 3 shows the proposed mechanism of the CNT growth during the CTS process. Under the high temperature of the CTS process, the metal salts will decompose [22, 23] (Figs. 3(i) and 3(ii))

$$M(NO_3)_x \xrightarrow{\triangle} M(l) + NO_z\uparrow \quad (1)$$

The formed metal nanoparticles will be in liquid phase and can move freely on the surface of CSF. There is surface-bound residual oxygen (O^*) on the CSF. CO_2 will form and release from the CSF surface because of carbon metabolism reaction (Fig. 3(iii))

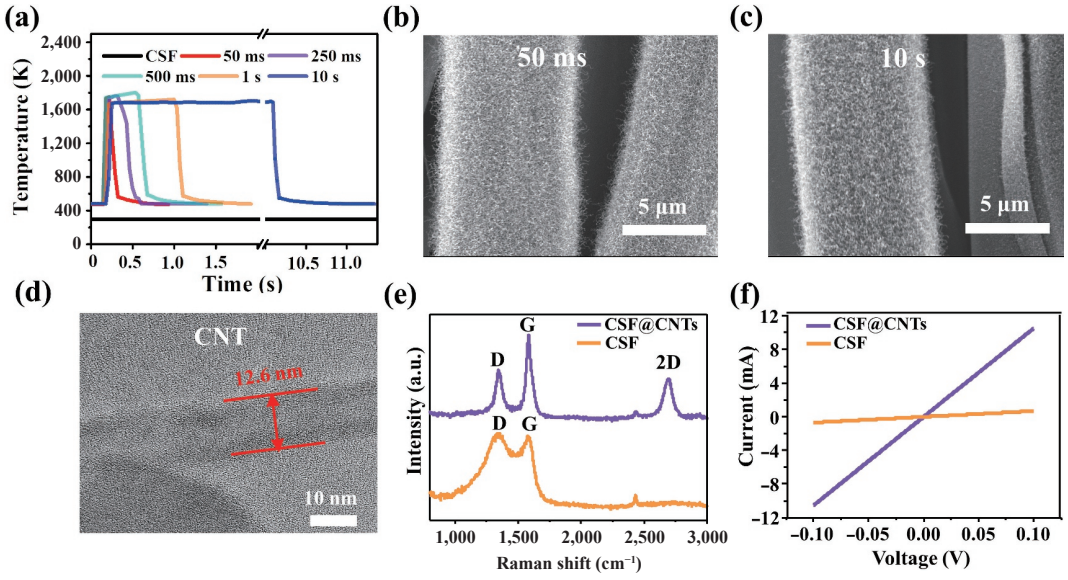

Figure 2 Characterization of CSF@CNTs synthesized through the CTS process. (a) The evolution of temperature with different CTS duration. (b) and (c) SEM images of CSF@CNTs with different CTS duration (50 ms and 10 s). (d) TEM image of the obtained CNT. (e) and (f) Raman spectra (e) and *I*–*V* curves (f) of the CSF and CSF@CNTs, respectively.

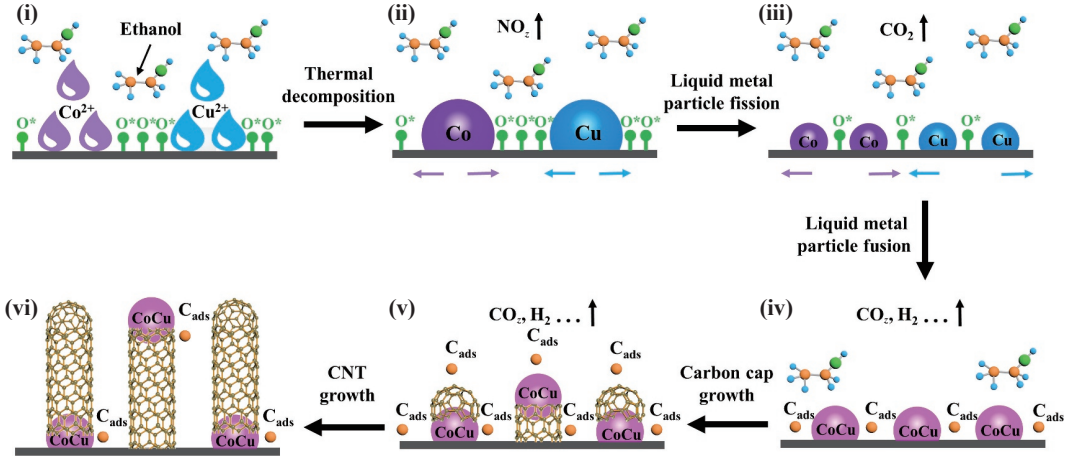

Figure 3 Schematic diagram illustrating the mechanism of CNT growth in the CTS process.

$$C + 2O^{*} \rightarrow CO_2\uparrow \quad (2)$$

Driven by the gas releasing, the liquid metal droplets will move quickly on the CSF surface and split ("fission"). The droplets with different compositions continually meet and fuse into single-phase CoCu alloy nanoparticles (Fig. 3(iv)), which serve as catalyst for the growth of CNTs.

At the same time, adsorbable carbon fragments (C_{ads}) form from the pyrolysis of ethanol and are absorbed on the CoCu nanoparticles, leading to the catalyzed growth of CNTs (Figs. 3(iv)–3(vi)). C_{ads} is a kind of activated carbon which is dissolved in the catalyst nanoparticles and the C_{ads} solubility gradually saturates to form a carbon cap [24], which then grows into CNTs. Both of tip growth mode and base growth mode were observed in this experiment using transmission electron microscopy (TEM) (Fig. S8 in the ESM). Since the CoCu nanoparticles are uniformly distributed on the CSF fibers, the CNTs are also uniformly grown on the surface of the CSF fibers, forming a fluffy structure.

Our experimental observations are consistent with the proposed mechanism. We find distinct CNT morphology through the same CTS process but only with CSFs processed at different carbonization temperatures (Fig. S9 in the ESM). We studied CSF carbonized at 1,073, 1,173, and 1,323 K, denoted as CSF-1073 K, CSF-1173 K, and CSF-1323 K, respectively. The O^{*} concentration of CSF decreases from 27.25% to 15.06% as the carbonization temperature rises from 1,073 to 1,323 K (Fig. S10 in the ESM). The smallest uniform catalyst nanoparticles and the best CNT morphology were obtained with CSF-1073 K among these samples, CSFs carbonized at different temperatures, indicating the O^{*} concentration of CSF play an important role for formation of small catalyst nanoparticles.

Furthermore, the decreased oxygen and nitrogen contents of CSF-1073K after the CTS process also verified the importance of O^{*} concentration. As shown in Fig. 4(a), the X-ray photoelectron spectroscopy (XPS) C 1s spectrum of CSF@CNTs exhibits lower C–N and C–O peaks than CSF. The O 1s and N 1s spectra show obviously decreased atomic concentrations of N and O after the CTS process (Figs. 4(b) and 4(c), and Fig. S11 in the ESM). During the CTS process, the high temperature provides sufficient energy for atom diffusion to break C–O and C–N bonds. These atoms recombine and release as gaseous products including CO_2, H_2O, and NO_z, as verified by thermogravimetric analysis–Fourier transform infrared (TA–FTIR) testing (Fig. 4(d)).

Besides, the cooling rate of the CTS (~ 10^5 K/s) is very high, which may avoid the solute partitioning process and thus enable the formation of solid solution structures. TEM image and the corresponding energy dispersive spectroscopy (EDS) elemental

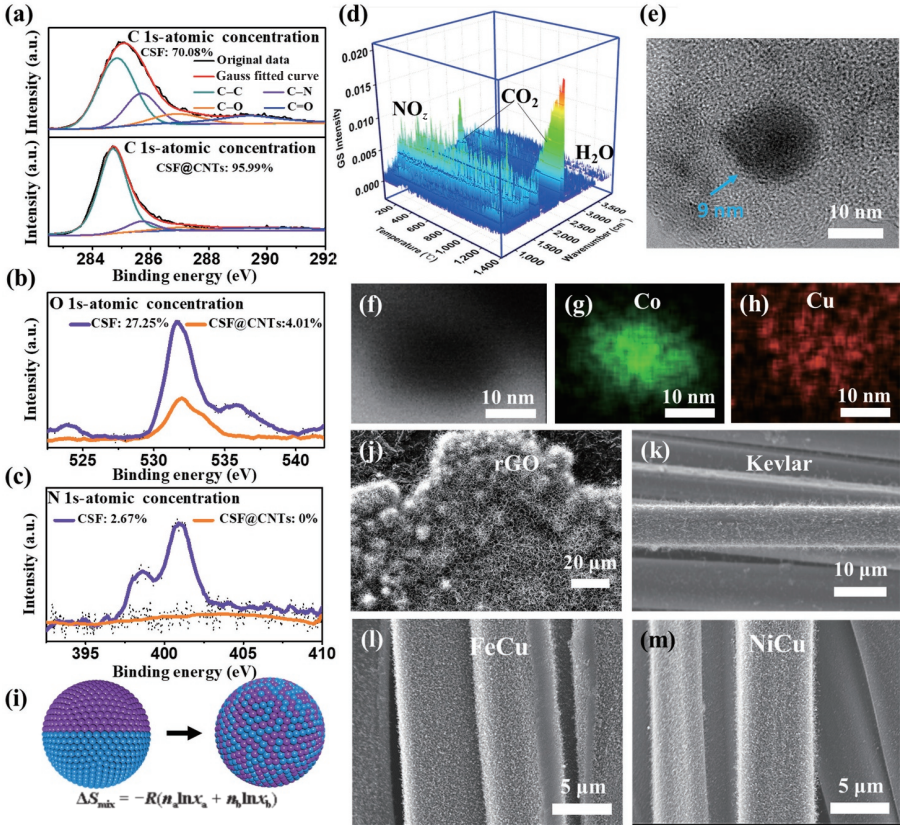

Figure 4 Experimental analysis on the mechanism of the CTS process and the growth of CNTs using other substrates and other catalysts. (a)–(c) High-resolution XPS C 1s, O 1s, and N 1s spectra of the CSF and CSF@CNTs. (d) TA–FTIR result of the CSF after loading metal salts. (e)–(h) TEM image (e) and elemental mapping images of Co and Cu of a CoCu nanoparticle (f)–(h). (i) Illustration showing a phase-separated heterostructure obtained by a conventional slow reduction procedure (left) and a solid-solution CoCu catalyst nanoparticle obtained by the CTS method (right). (j) and (k) CNTs grew on the rGO film (j) and carbonized Kevlar textile (k) through the CTS process. (l) and (m) SEM images of CNTs catalyzed by FeCu (l) and NiCu (m) catalysts.

mapping confirm the uniform distributions of Co and Cu in the CoCu alloy nanoparticles (Figs. 4(e)–4(h), Fig. S12 and Table S1 in the ESM). Figure 4(i) illustrates a phase-separated CoCu nanoparticle (in the equilibrium state that is usually formed in slow rate processes) and a solid-solution CoCu catalyst nanoparticle (in the nonequilibrium state that can be formed in fast kinetic processes). The formation of solid solution CoCu in the CTS process is favorable considering the mixing entropy (ΔS_{mix}).

The facile growth of CNTs through the CTS process can also be applied with other carbon substrates and other metallic catalysts. We observed that fluffy CNTs could grow on reduced graphene oxide (rGO) film (Fig. 4(j)) and carbonized Kevlar textile (Fig. 4(k)) with the CTS process. Besides, we show the growth of CNTs through the CTS process with FeCu (Fig. 4(l)) and NiCu catalyst (Fig. 4(m)). These results indicate that the CTS method may also be applied in synthesizing of other nanomaterials which require high temperature processes.

Furthermore, we demonstrate potential applications of the as-obtained CSF@CNTs textile. The textile has a similar fluffy structure with the spider's trichobothrium (a kind of fluff that senses outside airflow), endowing it with potential for highly sensitive airflow detection and high efficient air filters. As proof of concepts, we fabricated an airflow sensor and an air filter using the CSF@CNTs. which showed an obvious change in current in response to airflow. Figure 5(a) illustrates the structure of the CSF@CNTs and its response to an airflow. The number of contact points between the fluffy CNTs will significantly increase under airflow and thus lead to change in electrical resistance. Figure 5(b) shows the relative change in current versus airflow velocity of the airflow sensor. It possesses a low detection limit and fast response (0.8 s, Fig. S13 in the ESM). Figures 5(c)–5(d) compare the structure and the filtration efficiency of bare CSF and fluffy CSF@CNTs while being used as air filters. The specific surface area of the CSF@CNTs (62.476 m^2/g) is nearly 7 times of that of the CSF (9.238 m^2/g) as verified by Brunner–Emmet–Teller (BET) testing (Fig. S14(a) in the ESM). Besides, defects can be observed on the surface of the CNTs using high-resolution TEM (Fig. S14(b) in the ESM). The fluffy CNTs grown on the CSF lead to a hierarchical structure and a large specific surface area, contributing to obviously improved filtration efficiency compared with bare CSF.

3 Conclusion

In conclusion, we developed a facile and ultra-fast CTS method to synthesize CNTs, which can be completed with a simple homemade setup in 50 ms. A CSF fabric loaded with metal salts in ethanol solution was used as the substrate. The high temperature (~ 1,700 K) for the CNT growth was achieved by rapid Joule heating (ramp rates on the order of 10^5 K/s) induced by a pulse voltage (40 V, 50 ms) applied on the CSF fabric. The solvent ethanol undergoes pyrolysis and serves as the carbon precursor. The CTS process leads to the formation of small catalyst nanoparticles uniformly distributed on the surface of the CSF fibers, which catalyze the growth of the fluffy CNTs. The growth mechanism was analyzed. We find that the ultrafast heating rate and O^* concentrations play critical roles in this process. Besides, the growth of CNTs on other substrates, such as rGO and carbonized Kevlar textile, or with other catalysts, is also demonstrated. Finally, we fabricated a highly sensitive airflow sensor and a high efficient air filter to demonstrate the potential

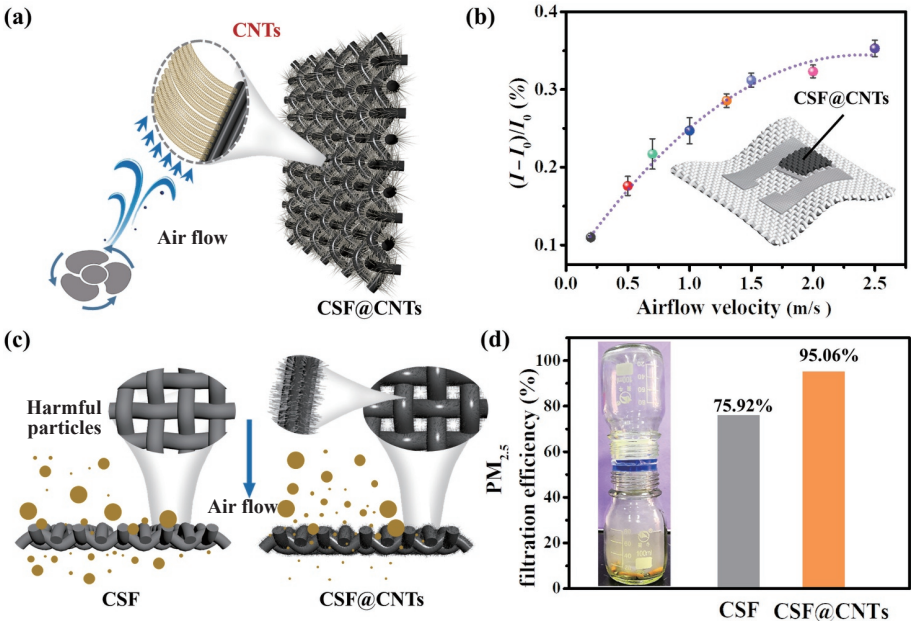

Figure 5 The applications of CSF@CNTs in airflow sensors and air filters. (a) Schematic illustration showing the working principle of the CSF@CNTs for sensing airflow. (b) Current variation ($(I - I_0)/I_0$ (%)) against airflow velocity of the CSF@CNTs airflow sensor. Inset is a schematic diagram of the flexible fabric-based CSF@CNTs airflow sensor. (c) Schematic illustration showing the difference of CSF and CSF@CNTs in air filtration. (d) $PM_{2.5}$ filtration efficiencies of a CSF filter and a CSF@CNTs filter. Inset is a photograph showing that a CSF@CNTs filter can block the diffusion of smoke from the bottom bottle to the top one.

applications of the unique fluffy CSF@CNTs textile. We foresee that the easy-accessible and highly efficient CTS approach will not only contribute to the research and manufacturing of CNTs, but also be applied for the facile growth of other nanomaterials.

4 Experimental

4.1 Preparation of carbon substrates and loading of metal salts

The CSF was synthesized according to our previous work [25]. Briefly, the fabrics were carbonized under an Ar (purity, 99.999%; gas flow, 100 standard cubic centimeters per minute (sccm)) and H_2 (purity, 99.999%; gas flow, 10 sccm) mixed atmosphere in a tube furnace with 1,073 K (unless otherwise noted). Similarly, the Kevlar textile was carbonized under 1,073 K. A rGO film was obtained through air pump filtration.

For ethanol-based metal salt solutions, the mixed ethanol solutions containing two kinds of metal salts (such as $Co(NO_3)_2$ and $Cu(NO_3)_2$, $Fe(NO_3)_3$ and $Cu(NO_3)_2$, or $Ni(NO_3)_2$ and $Cu(NO_3)_2$; 25 mM for each metal element) were directly dropped onto suspended CSF with loading of 60 μL/cm^2. It is worth noting that the ethanol solution containing a monometallic salt (such as $Co(NO_3)_2$ or $Cu(NO_3)_2$) was also directly dropped onto the suspended CSF with the loading of 60 μL/cm^2 (Fig. S15 in the ESM).

4.2 CTS process

The precursor-loaded sample was exposed in an Ar-filled plastic storage box (polypropylene, 22 cm × 14 cm × 16 cm) purchased from a supermarket. The CSF mentioned above was suspended on two Al_2O_3 slides and its two ends were connected to copper electrodes with silver paste. Then, the CSF was fast heated to a high temperature while applying a pulse voltage of 40 V for different durations (from 50 ms to 10 s). The pulse voltage was applied through an electric power source (Keithley 2680).

4.3 Characterization

The samples were characterized using SEM (FEI Quanta 650) and TEM (JEM 2010). Raman spectra were recorded using a Raman spectroscope (Horiba HR800, 532 nm). XPS was carried out by PHI Quantera SXM (ULVAC-PHI) scanning X-ray photoelectron spectrometer microprobe. The temperature of the samples was recorded using a laser temperature gun. The TA–FTIR result of CSF after loading metal salts was measured by TA–FTIR spectroscopy (NETZSCH, X70).

Acknowledgements

This work was financially supported by the National Key Technology R&D Program of China (No. 2020YFA0210702), and the National Natural Science Foundation of China (No. 21975141).

Electronic Supplementary Material: Supplementary material (photos, graphs, schemes, SEM, and TEM images; Raman and XPS spectra; EDS elemental analysis; atomic concentration table) is available in the online version of this article at https://doi.org/10.1007/s12274-021-3762-8.

References

[1] Zhang, Y. Y.; Zou, G. F.; Doorn, S. K.; Htoon, H.; Stan, L.; Hawley, M. E.; Sheehan, C. J.; Zhu, Y. T.; Jia, Q. X. Tailoring the morphology of carbon nanotube arrays: From spinnable forests to undulating foams. *ACS Nano* **2009**, *3*, 2157–2162.

[2] Lima, M. D.; Li, N.; De Andrade, M. J.; Fang, S. L.; Oh, J.; Spinks, G. M.; Kozlov, M. E.; Haines, C. S.; Suh, D.; Foroughi, J. et al. Electrically, chemically, and photonically powered torsional and tensile actuation of hybrid carbon nanotube yarn muscles. *Science* **2012**, *338*, 928–932.

[3] De Volder, M. F. L.; Tawfick, S. H.; Baughman, R. H.; Hart, A. J. Carbon nanotubes: Present and future commercial applications. *Science* **2013**, *339*, 535–539.

[4] Yang, Z. B.; Ren, J.; Zhang, Z. T.; Chen, X. L.; Guan, G. Z.; Qiu, L. B.; Zhang, Y.; Peng, H. S. Recent advancement of nanostructured carbon for energy applications. *Chem. Rev.* **2015**, *115*, 5159–5223.

[5] Wang, H. M.; Wang, C. Y.; Jian, M. Q.; Wang, Q.; Xia, K. L.; Yin, Z.; Zhang, M. C.; Liang, X. P.; Zhang, Y. Y. Superelastic wire-shaped supercapacitor sustaining 850% tensile strain based on

carbon nanotube@graphene fiber. *Nano Res.* **2018**, *11*, 2347–2356.
[6] Deng, J.; Li, J. F.; Chen, P. N.; Fang, X.; Sun, X. M.; Jiang, Y. S.; Weng, W.; Wang, B. J.; Peng, H. S. Tunable photothermal actuators based on a pre-programmed aligned nanostructure. *J. Am. Chem. Soc.* **2016**, *138*, 225–230.
[7] Wang, H. M.; Yang, Y.; Zhang, M. C.; Wang, Q.; Xia, K. L.; Yin, Z.; Wei, Y.; Ji, Y.; Zhang, Y. Y. Electricity-triggered self-healing of conductive and thermostable vitrimer enabled by paving aligned carbon nanotubes. *ACS Appl. Mater. Interfaces* **2020**, *12*, 14315–14322.
[8] Kim, S. H.; Haines, C. S.; Li, N.; Kim, K. J.; Mun, T. J.; Choi, C.; Di, J. T.; Oh, Y. J.; Oviedo, J. P.; Bykova, J. et al. Harvesting electrical energy from carbon nanotube yarn twist. *Science* **2017**, *357*, 773–778.
[9] Wang, H. M.; Li, S.; Wang, Y. L.; Wang, H. M.; Shen, X. Y.; Zhang, M. C.; Lu, H. J.; He, M. S.; Zhang, Y. Y. Bioinspired fluffy fabric with *in situ* grown carbon nanotubes for ultrasensitive wearable airflow sensor. *Adv. Mater.* **2020**, *32*, 1908214.
[10] Wang, H. M.; He, M. S.; Zhang, Y. Y. Carbon nanotube films: Preparation and application in flexible electronics. *Acta Phys.-Chim. Sin.* **2019**, *35*, 1207–1223.
[11] Shi, Z. J.; Lian, Y. F.; Zhou, X. H.; Gu, Z. N.; Zhang, Y. G.; Iijima, S.; Zhou, L. X.; Yue, K. T.; Zhang, S. L. Mass-production of single-wall carbon nanotubes by arc discharge method. *Carbon* **1999**, *37*, 1449–1453.
[12] Iijima, S. Helical microtubules of graphitic carbon. *Nature* **1991**, *354*, 56–58.
[13] Yudasaka, M.; Komatsu, T.; Ichihashi, T.; Iijima, S. Single-wall carbon nanotube formation by laser ablation using double-targets of carbon and metal. *Chem. Phys. Lett.* **1997**, *278*, 102–106.
[14] Zhang, S. C.; Hu, Y.; Wu, J. X.; Liu, D.; Kang, L. X.; Zhao, Q. C.; Zhang, J. Selective scission of C−O and C−C bonds in ethanol using bimetal catalysts for the preferential growth of semiconducting SWNT arrays. *J. Am. Chem. Soc.* **2015**, *137*, 1012–1015.
[15] Zhang, S. C.; Kang, L. X.; Wang, X.; Tong, L. M.; Yang, L. W.; Wang, Z. Q.; Qi, K.; Deng, S. B.; Li, Q. W.; Bai, X. D. et al. Arrays of horizontal carbon nanotubes of controlled chirality grown using designed catalysts. *Nature* **2017**, *543*, 234–238.
[16] He, M. S.; Chernov, A. I.; Obraztsova, E. D.; Jiang, H.; Kauppinen, E. I.; Lehtonen, J. Synergistic effects in FeCu bimetallic catalyst for low temperature growth of single-walled carbon nanotubes. *Carbon* **2013**, *52*, 590–594.
[17] He, M. S.; Chernov, A. I.; Fedotov, P. V.; Obraztsova, E. D.; Sainio, J.; Rikkinen, E.; Jiang, H.; Zhu, Z.; Tian, Y.; Kauppinen, E. I. et al. Predominant (6,5) single-walled carbon nanotube growth on a copper-promoted iron catalyst. *J. Am. Chem. Soc.* **2010**, *132*, 13994–13996.
[18] He, M. S.; Liu, B. L.; Chernov, A. I.; Obraztsova, E. D.; Kauppi, I.; Jiang, H.; Anoshkin, I.; Cavalca, F.; Hansen, T. W.; Wagner, J. B. et al. Growth mechanism of single-walled carbon nanotubes on iron-copper catalyst and chirality studies by electron diffraction. *Chem. Mater.* **2012**, *24*, 1796–1801.
[19] Yao, Y. G.; Huang, Z. N.; Xie, P. F.; Lacey, S. D.; Jacob, R. J.; Xie, H.; Chen, F. J.; Nie, A. M.; Pu, T. C.; Rehwoldt, M. et al. Carbothermal shock synthesis of high-entropy-alloy nanoparticles. *Science* **2018**, *359*, 1489–1494.
[20] Neuer, G. Spectral and total emissivity measurements of highly emitting materials. *Int. J. Thermophys.* **1995**, *16*, 257–265.
[21] Yao, Y. G.; Fu, K. K.; Zhu, S. Z.; Dai, J. Q.; Wang, Y. B.; Pastel, G.; Chen, Y. N.; Li, T.; Wang, C. W.; Li, T. et al. Carbon welding by ultrafast Joule heating. *Nano Lett.* **2016**, *16*, 7282–7289.
[22] Dollimore, D.; Griffiths, D. L.; Nicholson, D. 488. The thermal decomposition of oxalates. Part II. Thermogravimetric analysis of various oxalates in air and in nitrogen. *J. Chem. Soc.* **1963**, 2617–2623.
[23] Sinha, A. S. K.; Shankar, V. Characterization and activity of cobalt oxide catalysts for total oxidation of hydrocarbons. *Chem. Eng. J.* **1993**, *52*, 115–120.
[24] He, M. S.; Zhang, S. C.; Wu, Q. R.; Xue, H.; Xin, B. W.; Wang, D.; Zhang, J. Designing catalysts for chirality-selective synthesis of single-walled carbon nanotubes: Past success and future opportunity. *Adv. Mater.* **2019**, *31*, 1800805.
[25] Wang, C. Y.; Li, X.; Gao, E. L.; Jian, M. Q.; Xia, K. L.; Wang, Q.; Xu, Z. P.; Ren, T. L.; Zhang, Y. Y. Carbonized silk fabric for ultrastretchable, highly sensitive, and wearable strain sensors. *Adv. Mater.* **2016**, *28*, 6640–6648.